CHARACTERIZATION OF SATURATED POROUS ROCKS WITH OBLIQUELY DIPPING FRACTURES

Jiao Xue and Robert H. Tatham

Department of Geological Sciences
The University of Texas at Austin

ABSTRACT

Elastic properties, fracture parameters and amplitude variation with offset and azimuth (AVOA) of fluid saturated porous media with obliquely dipping fractures are studied. Effective stiffness and anisotropy parameters for porous media with vertical fractures are studied using Gassmann equations for linear-slip theory and fractured models developed by Hudson and Thomsen. Linear-slip theory and Hudson's model for penny-shaped cracks can be used to relate the anisotropic parameters to the fracture properties. Considering porous rocks with saturated penny-shaped cracks and hydraulically connected cracks and pores, normal and tangential weakness of the fractures are related to fluid factor, and can be obtained by making the anisotropic parameters for linear-slip model be identical to anisotropic parameters given by Thomsen. The effect of fluid infill on elastic properties is investigated. Using Bond transformation, the stiffness matrix of the dipping fractured medium can be obtained. Then, characterization of fluid saturated porous rocks with obliquely dipping fractures is investigated, and variation of reflection coefficients as a function of azimuth and incidence angle is analyzed. For the saturated porous rocks with obliquely dipping fractures, the effect of porosity, fluid infill and dipping angle on horizontal and vertical velocities, anisotropic parameters and reflection coefficients are examined. In the end, we estimated the dip of dipping fractures by AVOA analysis, and obtained fracture parameters from synthetic reflection data. Results show that this estimation method yields dip angle with reasonable accuracy, and inversion results are consistent with the model. Our ultimate goal is to invert seismic data for the physical characteristics of fractures, and host rocks.

INTRODUCTION

In seismic exploration, characterization of naturally fractured hydrocarbons reservoirs is of great interest. It is known that the orientation of fractures makes the medium azimuthally anisotropic. The simplest effective model of a fractured reservoir is transversely isotropic media with a horizontal symmetry axis (HTI), resulting from rotationally invariant vertical fracture sets contained in isotropic host rock.

Three kinds of effective models of fractured and porous media are discussed, including models with thin and highly compliant layers or planes of weakness with linear-slip boundary conditions (Schoenberg, 1980, 1983), isolated parallel penny-shaped cracks (Hudson, 1980, 1981), and hydraulically connected cracks and pores (Thomsen, 1995). Schoenberg and Douma (1988) pointed out that the model with infinite parallel fractures with linear-slip boundary (Schoenberg, 1980, 1983) and penny-shaped crack model have the same structure of effective stiffness. Bakulin (2000) demonstrated that even the presence of equant pores which are hydraulically connected to the fractures and cracks does not change the structure of stiffness tensor.

Not all naturally fracture sets are vertical or near-vertical orientated. Over the last decades, there is growing studies about the obliquely dipping fractures, which may have been tilted away from the vertical because of the oblique stresses and other factors (Angerer et al. 2002). Grechka and Tsvankin (2004) investigated the characterization of obliquely dipping fractures in transversely isotropic background, including effective stiffness matrix, phase velocities and polarizations, NMO velocities in such media, and inversion of seismic data for the fracture and background parameters. Shaw and Sen (2004) derived the lineared reflection coefficient for a weakly triclinic medium underlying an isotropic medium.

Fluid effect on seismic characteristics has also attracted increasing interest in reservoir characterization. Isotropic Gassmann (1995) equation is widely used to study the fluid effect in isotropic porous reservoirs. Gurevich (2003) modeled the elastic properties of saturated fractured and porous medium, by combining the linear-slip theory (Schoenberg and Douma, 1988; Schoenberg, 1980, 1983) and Gassmann (1995) equations. Sil and Sen (2011) analyzed the effect of fluid substitution on elastic properties (e.g., P-wave moduli, horizontal and vertical velocities, anisotropic parameters and reflection coefficients).

We proposed a combination of linear-slip theory (Schoenberg, 1980, 1983) and hydraulically connected fractured and porous model given by Thomsen (1995), and a combination of a general linear-slip theory and elastic properties given by Gurevich (2003). For the saturated fractured medium with background porosity, the compliance matrix can not be simply written as the sum of compliance of an isotropic host rock and excess normal and tangential compliance associated with the fractures. However, we can still take the compliance matrix as a difference between the compliance matrix of the saturated fractured and porous medium and the saturated host rock. Here, we investigate the fracture weakness in different directions, and represent the stiffness matrix as sum of the saturated elastic constants and normal fracture weakness on different directions. Assuming the fractures are dipping, we investigated the reflection coefficients variation with incidence angle and azimuth.

METHODOLOGY

Gurevich (2003) derived the exact static elastic moduli of a fluid-saturated fractured and porous rock based on Gassmann's anisotropic fluid substitution equations. According to Gassmann's equations, the elastic modulus of a fluid-saturated porous rock with fractures can be obtained by summing the elastic modulus of the dry fractured and porous rock and an additional fluid effect term.

Saturated porous medium with vertical fractures

The dry fractured and porous rock can be assumed as a spatially homogeneous and isotropic porous host rock permeated by a set of parallel vertical fractures (Gurevich, 2003), and can be treated as transversely isotropic medium with a horizontal axis of symmetry (HTI). The dry stiffness matrix with rotationally invariant fractures parallel to y-z plane can be expressed (Schoenberg and Sayers, 1995) as

$$C_{dry}^{0}(HTI)=\begin{bmatrix} L(1-\Delta N) & \lambda(1-\Delta N) & \lambda(1-\Delta N) & & & \\ \lambda(1-\Delta N) & L(1-r^2\Delta N) & \lambda(1-\Delta N) & & & \\ \lambda(1-\Delta N) & \lambda(1-\Delta N) & L(1-r^2\Delta N) & & & \\ & & & \mu & & \\ & & & & \mu(1-\Delta T) & \\ & & & & & \mu(1-\Delta T) \end{bmatrix} \tag{1}$$

where,

$$L=\lambda+2\mu \quad , \tag{2}$$

$$r=\frac{\lambda}{\lambda+2\mu} \ , \tag{3}$$

$$\Delta_N=\frac{(\lambda+2\mu)K_N}{1+(\lambda+2\mu)K_N}, \text{ and} \tag{4}$$

$$\Delta_T=\frac{\mu K_T}{1+\mu K_T}. \tag{5}$$

In above equations, λ and μ are Lame constants, K_N and K_T are the normal and tangential excess fracture compliances, and Δ_N and Δ_T normal and tangential fracture weakness (Schoenberg and Sayers, 1995).

Gurevich (2003) derived the stiffness elements of a fluid-saturated fractured rock using Gassmann's equation, which is not related to the shape of the pores or fractures:

$$C_{11}^{sat} = \frac{L}{D}\left\{ d_1\theta + \frac{K_f}{\varphi K_g L}\left[L_1\alpha' - \frac{16\mu^2\alpha_0\Delta N}{9L} \right] \right\}, \tag{6}$$

$$C_{33}^{sat} = \frac{L}{D}\left\{ d_2\theta + \frac{K_f}{\varphi K_g L}\left[L_1\alpha' - \frac{4\mu^2\alpha_0\Delta N}{9L} \right] \right\}, \tag{7}$$

$$C_{13}^{sat} = \frac{\lambda}{D}\left\{ d_1\theta + \frac{K_f}{\varphi K_g \lambda}\left[\lambda_1\alpha' + \frac{8\mu^2\alpha_0\Delta N}{9L} \right] \right\}, \tag{8}$$

$$C_{44}^{sat} = \mu, \text{ and} \tag{9}$$

$$C_{55}^{sat} = \mu(1-\Delta T). \tag{10}$$

where,

$$D = 1 + \frac{K_f}{K_g\varphi}(\alpha_0 - \varphi + \frac{K^2\Delta N}{K_g L}), \tag{11}$$

$$\theta = 1 - \frac{K_f}{K_g}, \tag{12}$$

$$\alpha_0 = 1 - \frac{K}{K_g}, \tag{13}$$

$$\alpha' = \alpha_0 + \frac{K^2}{K_g L}\Delta N, \tag{14}$$

$$L_1 = K_g + \frac{4}{3}\mu, \tag{15}$$

$$\lambda_1 = K_g - \frac{2}{3}\mu, \tag{16}$$

$$d_1 = 1 - \Delta N\,, \tag{17}$$

$$d_2 = 1 - \frac{\lambda^2}{L^2}\Delta N\,, \tag{18}$$

In the above equations, φ is the porosity, and K, K_g and K_f are bulk modulus of the dry host rock, solid grain and fluid, respectively.

The stiffness matrix of Schoenberg's linear-slip model and Hudson's isolated penny-shaped fracture model have the same structure and can be identical if the fracture weakness satisfy the relationships given by Schoenberg and Douma (1988):

$$\Delta N = \frac{4e}{3g(1-g)\left[1 + \frac{1}{\pi g(1-g)a}\frac{K_f + 4/3\mu_f}{\mu}\right]}, \tag{19}$$

$$\Delta T = \frac{16e}{3(3-2g)\left[1 + \frac{4}{\pi(3-2g)a}\left(\frac{\mu_f}{\mu}\right)\right]}. \tag{20}$$

where, $g = \frac{\mu}{L}$. μ_f is shear modulus of the infill material, and e is the crack density, and can be expressed by crack porosity φ_C and aspect ratio a of the spheroidal crack:

$$e = \frac{3\varphi_C}{4\pi a} \tag{21}$$

For dry porous and fractured medium ($K_f = \mu_f$ =0) in equation 1,

$$\Delta N = \frac{4e}{3g(1-g)}, \text{ and} \tag{22}$$

$$\Delta T = \frac{16e}{3(3-2g)}. \tag{23}$$

The compliance matrix for the saturated fractured medium with equant porosity can no longer be represented as the sum of isotropic host rock and an excess normal and tangential compliance related to the fractures. However, we can still obtain the excess compliance due to fractures as a difference between the compliance matrix of the saturated fractured and porous model and the isotropic background. In this condition, we assume the saturated stiffness matrix can be written in the form of

$$C^{sat} = \begin{bmatrix} L^{sat}(1-\Delta N_{11}^{sat}) & \lambda^{sat}(1-\Delta N_{13}^{sat}) & \lambda^{sat}(1-\Delta N_{13}^{sat}) & & & \\ \lambda^{sat}(1-\Delta N_{13}^{sat}) & L^{sat}(1-r_{sat}{}^{2}\Delta N_{33}^{sat}) & \lambda^{sat}(1-r_{sat}\Delta N_{23}^{sat}) & & & \\ \lambda^{sat}(1-\Delta N_{13}^{sat}) & \lambda^{sat}(1-r_{sat}\Delta N_{23}^{sat}) & L^{sat}(1-r_{sat}{}^{2}\Delta N_{33}^{sat}) & & & \\ & & & \mu & & \\ & & & & \mu(1-\Delta T) & \\ & & & & & \mu(1-\Delta T) \end{bmatrix} \quad (24)$$

Following Bakulin (2000), we assume the equant porosity is small, and the Thomsen anisotropic parameter in Thomsen's hydraulically connected fractured and porous model can be given as

$$\varepsilon = 2g(1-g)\Delta N^{\mathrm{T\,hom\,sen}}. \quad (25)$$

$$\text{Thus, } \Delta N^{\mathrm{T\,hom\,sen}} = \frac{4}{3}\frac{e}{g(1-g)}\left(1-\frac{K_f}{K_g}\right)D_{cp}. \quad (26)$$

Dcp is fluid factor, and is given (Thomsen, 1995) as

$$D_{cp} = \left[1-\frac{Kf}{Kg}+\frac{Kf}{Kg(\varphi_c+\varphi_p)}\left(\frac{3-2g}{2g}\varphi_p+\frac{4(2-3g)}{9(1-g)}e\right)\right]^{-1}. \quad (27)$$

The weakness ΔN in equation 19 and equation 22 are for dry and isolated fluid-filled cracks, respectively. If the fluid can escape into the hydraulically connected pores from the fractures under stress, fracture weakness $\Delta N^{\mathrm{T\,hom\,sen}}$ must be between zero and the fracture weakness for dry or gas-filled cracks. Here, we made an assumption that the stiffness matrix can be expressed in the form of equation 1.

Reflection variation with incidence angle and azimuth

Amplitude variation with offset (AVO) can be described by Thomsen type anisotropic parameters $\varepsilon^{(V)}$, $\delta^{(V)}$ and γ, The linearized reflection coefficient for a fractured reservoir with vertical fractures and isotropic overburden can be expressed as (Ruger, 1998)

$$R_{PP}^{HTI}(i,\phi) = {}^{iso}R_{PP}^{HTI}(i) + {}^{ani}R_{PP}^{HTI}(i,\phi) \quad (28)$$

$${}^{iso}R_{PP}^{HTI}(i) = \frac{1}{2}\frac{\Delta Z}{Z_0}+\frac{1}{2}\left[\frac{\Delta\alpha}{\alpha_0}-4\left(\frac{\beta_0^2}{\alpha_0^2}\right)\frac{\Delta G}{G_0}\right]\sin^2 i+\frac{1}{2}\frac{\Delta\alpha}{\alpha_0}\sin^2 i\tan^2 i \quad (29)$$

$$
\begin{aligned}
{}^{ani}R_{PP}^{HTI} &= \frac{1}{2}\left[\Delta\delta^{(V)} + 8\frac{\beta_0^2}{\alpha_0^2}\Delta\gamma\right]\cos^2\phi\sin^2 i \\
&+ \frac{1}{2}\left[\Delta\varepsilon^{(V)}\cos^4\phi + \Delta\delta^{(V)}\sin^2\phi\cos^2\phi\right]\sin^2 i\tan^2 i
\end{aligned}
\tag{30}
$$

Here, i is the incident angle, and ϕ is azimuth angle, which is the angle between the observation line and the symmetry axis of the fractures. α_0 and β_0 are velocities of the vertical P-wave and shear wave that is polarized on the isotropic plane. Z_0 and G_0 are P-wave impendence and shear modulus of the background medium. $\varepsilon^{(V)}$, $\delta^{(V)}$ and γ are Thomsen-type parameters, and Δ indicating weak contrast between the upper and lower layers across the interface.

$$
\begin{aligned}
&{}^{ani}R_{PP}^{HTI}(\phi,i) - {}^{ani}R_{PP}^{HTI}(\phi+\pi/2,i) \\
&= \frac{1}{2}\left[\Delta\delta^{(V)} + 8\frac{\beta_0^2}{\alpha_0^2}\Delta\gamma\right]\left(\cos^2\phi - \sin^2\phi\right)\sin^2 i + \frac{1}{2}\Delta\varepsilon^{(V)}\left(\cos^2\phi - \sin^2\phi\right)\sin^2 i\tan^2 i
\end{aligned}
\tag{31}
$$

Shaw and Sen (2004) give the linearized reflection coefficient for a fractured reservoir with dipping fractures and isotropic overburden,

$$
\begin{aligned}
{}^{ani}R_{PP}^{TTI} &= \left[\frac{\Delta\delta^{(V)}}{2}\left(\cos^2\psi - \sin^2\theta\right) - \left(\Delta\varepsilon^{(V)} - \Delta\delta^{(V)}\right)\left(\cos^2\psi + \sin^2\theta\right)\sin^2\theta + 4\frac{\beta_0^2}{\alpha_0^2}\gamma\cos^2\psi\right]\sin^2 i \\
&+ \frac{1}{2}\left[\Delta\delta^{(V)}\left(\cos^2\psi - \sin^2\theta\right) + \left(\Delta\varepsilon^{(V)} - \Delta\delta^{(V)}\right)\left(\cos^4\psi + \sin^4\theta\right)\right]\sin^2 i\tan^2 i
\end{aligned}
\tag{32}
$$

Here, $\cos\psi = \cos\theta^0\cos\phi$ with θ^0 representing the dip angle of the fractures.

For the dry fractured porous rock,

$$\varepsilon^{(V)} \approx -2g(1-g)\Delta N \tag{33}$$

$$\delta^{(V)} \approx -2g\left[(1-2g)\Delta N + \Delta T\right] \tag{34}$$

$$\gamma \approx \frac{\Delta T}{2} \tag{35}$$

The effect of fracture density and fluid infill on elastic properties of the fractured porous rocks with vertical and obliquely dipping fractures and AVOA are studied.

SYNTHETIC EXAMPLES AND RESULTS

One of our goals of this investigation is to analyze the effect of fracture density, crack infill, and porosity of the background rock on the fracture weakness for different fractured models. We consider a fractured tight-gas sandstone model documented by Mavko et al. (2003). The properties of the tight gas-sandstone are shown in Table 1.

Table 1. Properties of tight gas-sandstone.

	P-wave velocity (km/s)	S-wave velocity (km/s)	Density (g/cm^3)	Porosity
Tight gas-sandstone	4.67	3.06	2.51	5%

Saturation: Dry.

Effective pressure: 40Mpa.

Date source: Jizba (1991)

Figure 1a shows the fracture weakness for the fractures with infill material of gas, oil and water using Thomsen's hydraulically connected model. Figure 1b is the fracture weakness using equation 24. It is obvious, the fracture weakness using Thomsen's hydraulically connected fractured and porous model are approximate to ΔN_{11}^{sat} in equation 24. In figure 1b, $\Delta N_{11}^{sat} \neq \Delta N_{13}^{sat} \neq \Delta N_{33}^{sat}$, which means that the stiffness matrix can not be written in the form of equation 1 for the saturated fractured and porous media. Thus the compliance matrix for the saturated fractured medium cannot be expressed as the sum of an isotropic saturated matrix and an excess compliance due to the fractures with fluid infill. Although the saturated fractured and porous medium cannot be described by two elastic constants of the background and two excess compliance of the fractures, it can be described by six parameters (λ, μ, ΔN_{11}^{sat}, ΔN_{13}^{sat}, ΔN_{33}^{sat}, and ΔT). As we can see in figure 1b, the fracture weaknesses for three directions are different for crack infill of gas, oil and water. The distribution of fracture weakness for different directions, especially, ΔN_{33}^{sat} may provide us a method to separate dry (or gas-filled) and fluid-filled cracks.

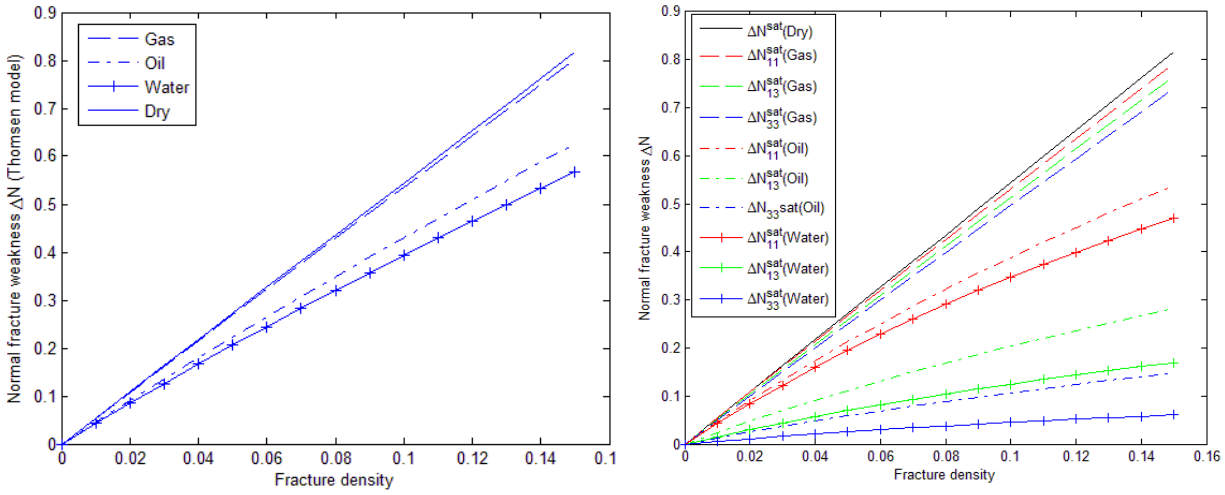

a) b)

Figure 1. a) Fracture weakness variation with fracture density using Thomen's hydraulically connected fractured and porous model. Assuming the equant porosity is small, and the stiffness matrix can be expressed in the form of equation 1. b) Fracture weakness in different directions variation with fracture density for fluid infill of gas, oil and water.

Figure 2 shows the effect of porosity of the background on the fracture weakness and anisotropy parameter ε. Figure 2a shows the normal fracture weakness variation with equant porosity. This normal fracture weakness is obtained using the saturated hydraulically connected fractured and porous model given by Thomsen. The normal weakness ΔN is zero for zero background porosity, and increases sharply within one or two percent porosity. The sharp increase of ΔN results from the fact that fluid factor increase sharply to 1, with the increase of equant porosity. Figure 2b shows similar increase in P-wave anisotropy parameter ε. As discussed by Thomsen (1995), the fluid in the fractures has plenty of space to escape to when the equant porosity increase from zero to a few percent, so the fracture will be as compliant as in the dry medium. Figure 2c shows the fracture weakness in different directions, and shows similar increase. However, the increase of ΔN_{33}^{sat} is small. We think it is because when compressed, the fluids in the vertical fractures may mainly escape horizontally to the surrounded pores. That is also why ΔN_{11}^{sat} increase sharply like the normal fracture weakness in Thomsen's model.

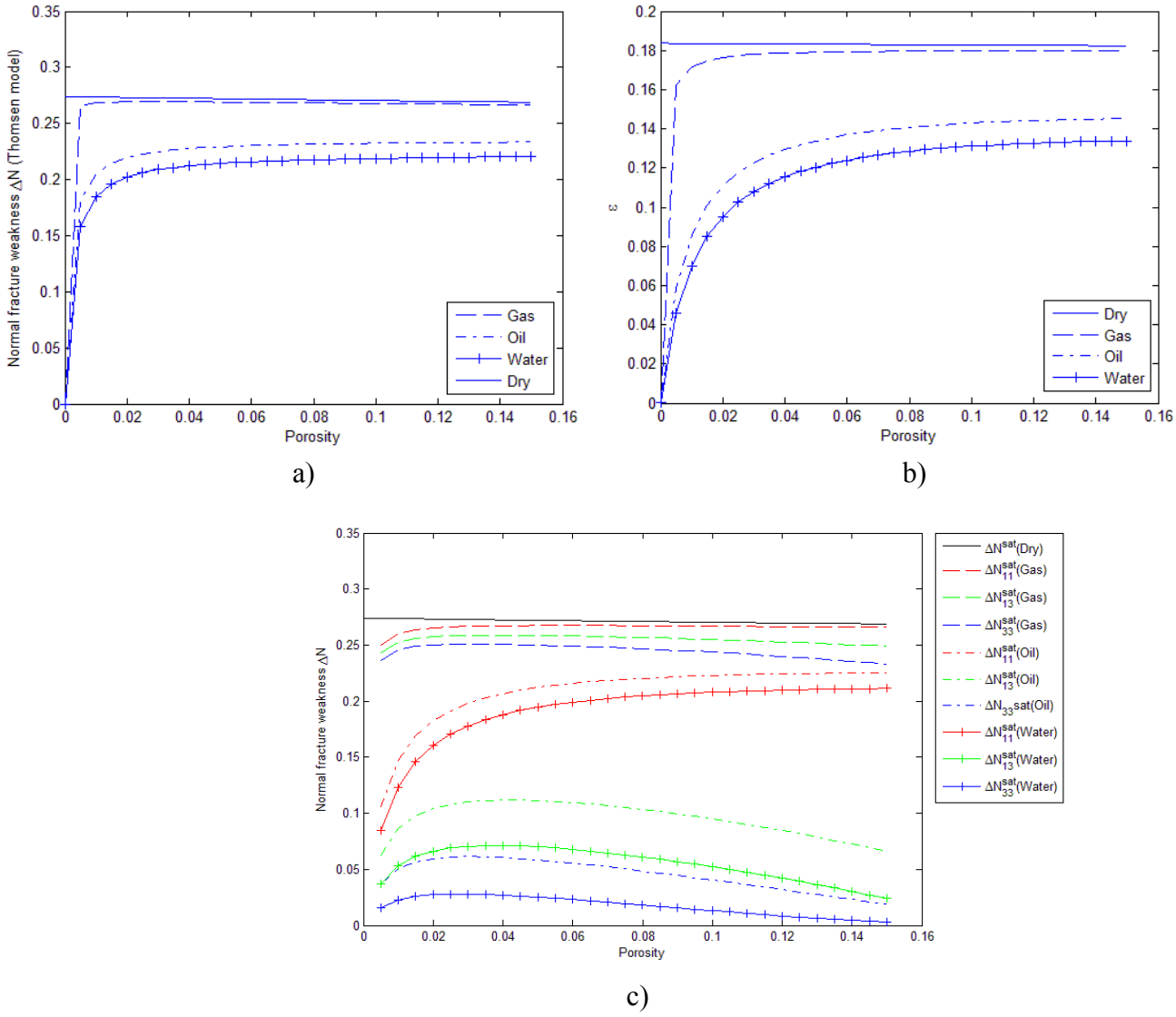

Figure 2. a) Fracture weakness variation with porosity using Thomen's hydraulically connected fractured and porous model. Assuming the equant porosity is small, and the stiffness matrix can be expressed in the form of equation 1. b) P-wave anisotropy parameter ε variation with porosity for fluid infill of gas, oil and water. c) Normal fracture weakness for different directions variation with porosity for fluid infill of gas, oil and water.

We also investigate the effect of porosity on horizontal and vertical P-wave velocity, for different fracture weakness. In figure 3b, the velocity decrease with the increase of fracture weakness. However, in figure 3a, the decrease is not obvious for the vertical P-wave velocity.

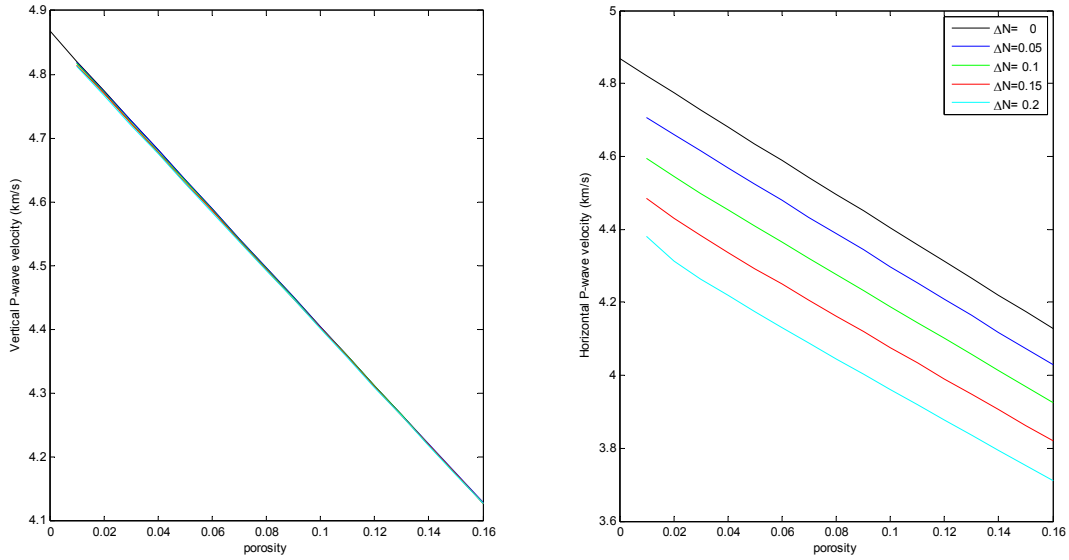

a) b)

Figure 3. a) Vertical and b) Horizontal velocity variation with porosity for different fracture weakness.

In order to investigate the reflection variation with incidence angle and azimuth, we consider a model with two layers (Table 2). The upper layer is isotropic water-saturated sandstone, and the lower layer in tight gas-sandstone containing obliquely dipping fractures. We assume the dip is 0°， 30°and 60°respectively. The reflection coefficients variation with incidence angle and azimuth is shown in figure 4a. Figure 4b shows the reflection coefficients variation with azimuth for dip angle of 0°, 30°and 60°, when the incidence angle is 30°.

Table 2. Properties of a two-layer model

	P-wave velocity (km/s)	S-wave velocity (km/s)	Density (g/cm^3)	ΔN	ΔT
Sandstone	4.09	2.41	2.37	0	0
Tight-gas sandstone	4.67	3.06	2.51	0.15	0.1

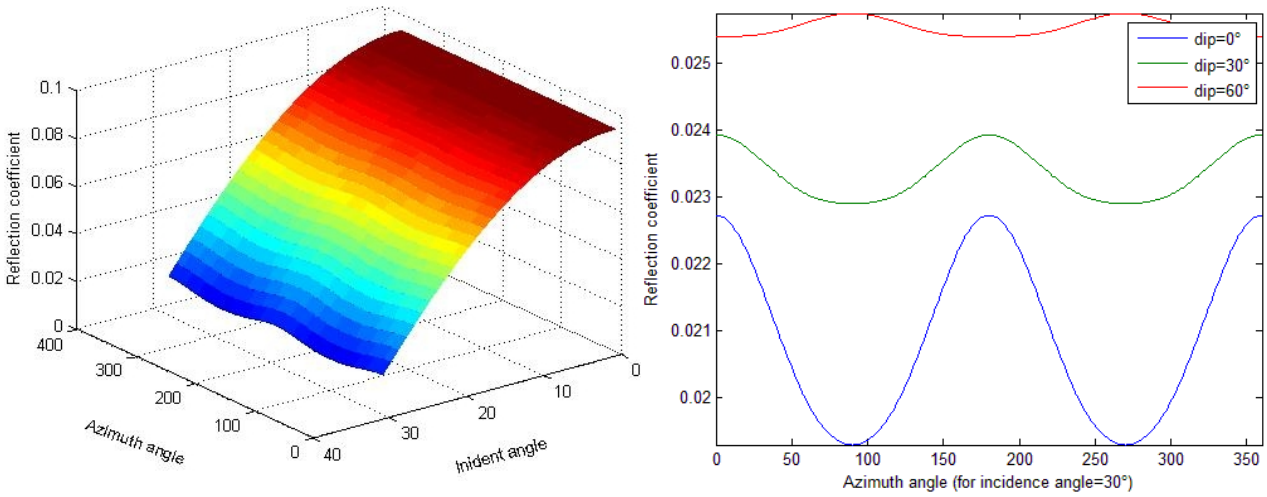

Figure 4. a) reflection coefficients variation with incidence angle and azimuth. b) reflection coefficients variation with azimuth for dip angle of 0°, 30°and 60°, when the incidence angle is 30°.

The effect of fluid on AVOA

We studied the effect of fluid on AVOA, by using a 100% water or gas saturated porous model with obliquely dipping fractures. The reason why we take the tight-gas sandstone as the upper layer, and take sandstone as the lower layer is that the porosity range of the tight-sandstone model documented by Mavko (2009) is 0~15%. In this work, we investigate reflection coefficients when the porosity is 10% and 25%, respectively. Given the physical properties of the dry fractured sandstone, $\varepsilon_{sat}^{(V)}$, $\delta_{sat}^{(V)}$, and γ_{sat} can be calculated.

Table 3. Properties of a two-layer model

	P-wave velocity (km/s)	S-wave velocity (km/s)	Density (g/cm^3)	ΔN	ΔT
Tight-gas sandstone	4.67	3.06	2.51	0	0
Sandstone	4.09	2.41	2.37	0.15	0.1

Figure 5a, 5c, 5e, and 5g illustrates the effect of porosity and fluid infill on amplitude variation with azimuth and incident angle for different dip angle. Dip=0°means that the fracture is vertical. Figure 5b, 5d, 5f, and 5h shows the reflection coefficient variation with azimuth angle for different dip angle, when the incident angle is 30°.

Small porosity of 10% and large porosity of 25% are considered in this case. For small incident angle, reflection coefficient variation with azimuth is almost not visible. This is because the fracture density here is small. The variation with azimuth is more visible for larger porosity. For the water saturated fractured porous model with porosity of 10%, reflection amplitude decrease with the increase of incident angle. However, for the gas saturated model with porosity of 25%, reflection amplitude increase with the increase of incident angle. For gas saturated fractured porous rock, we obtained the same result. An increase in the equant porosity changes the trends of the reflection coefficients variation with incidence angle.

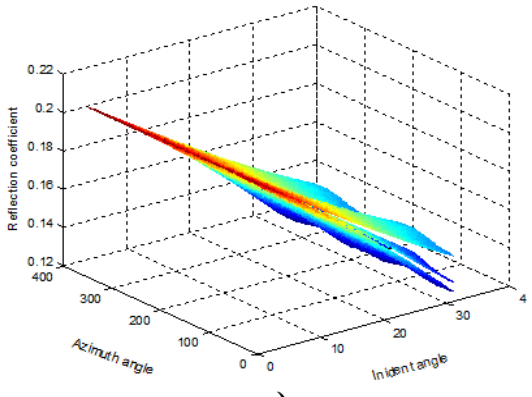
Reflection coefficient
Azimuth angle
Incident angle

a)

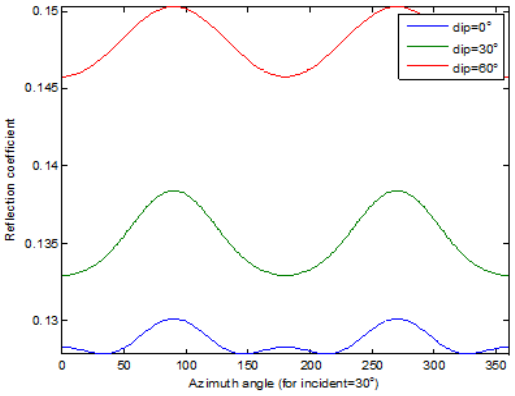
dip=0°
dip=30°
dip=60°
Reflection coefficient
Azimuth angle (for incident=30°)

b)

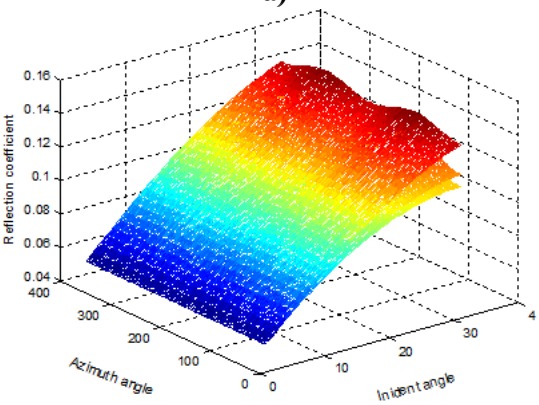
Reflection coefficient
Azimuth angle
Incident angle

c)

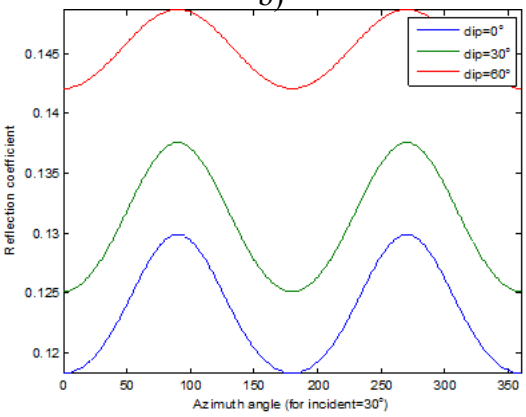
dip=0°
dip=30°
dip=60°
Reflection coefficient
Azimuth angle (for incident=30°)

d)

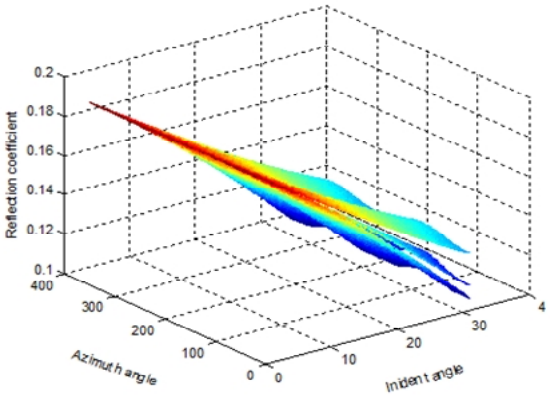
Reflection coefficient
Azimuth angle
Incident angle

e)

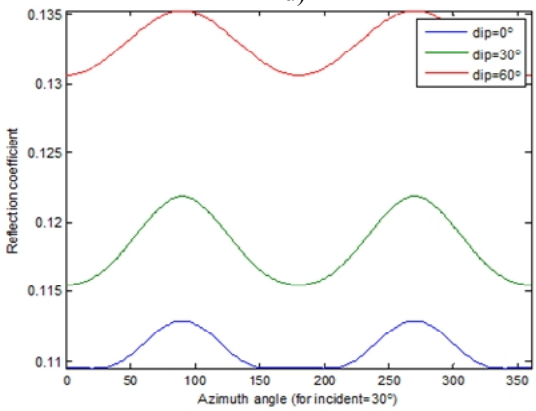
dip=0°
dip=30°
dip=60°
Reflection coefficient
Azimuth angle (for incident=30°)

f)

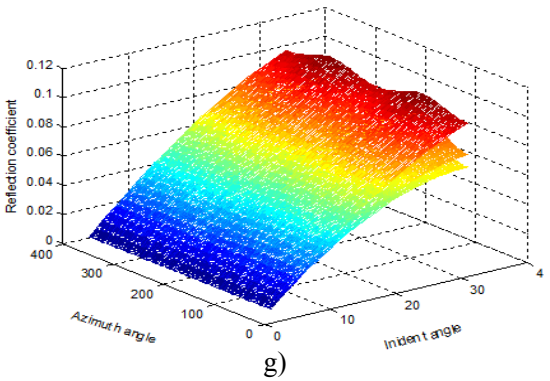
Reflection coefficient
Azimuth angle
Incident angle

g)

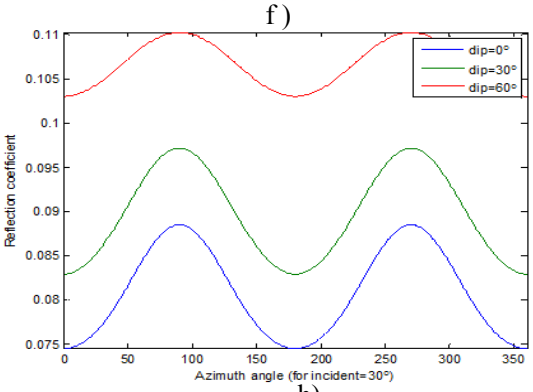
dip=0°
dip=30°
dip=60°
Reflection coefficient
Azimuth angle (for incident=30°)

h)

Figure 5. Reflection coefficients variation with incidence angle and azimuth for a) water saturated fractured model with porosity of 10%, c) water saturated fractured model with porosity of 25%, e) gas saturated fractured model with porosity of 10%, and g) gas saturated fractured model with porosity of 25%; reflection coefficients variation with azimuth for dip angle of 0°, 30°and 60°, when the incidence angle is 30°for b) water saturated fractured model with porosity of 10%, d) water saturated fractured model with porosity of 25%, f) gas saturated fractured model with porosity of 10%, and h) gas saturated fractured model with porosity of 25%.

CONCLUSIONS

We proposed a combination of linear-slip theory (Schoenberg, 1980, 1983) and hydraulically connected fractured and porous model given by Thomsen (1995). For small equant porosity, we investigate the hydraulically connected fractured and porous model given by Thomsen. Assuming the compliance matrix for small equant porosity can be expressed by the sum of an isotropic matrix of the saturated host rock and an excess compliance, we can derive the fracture weakness for the hydraulically connected fractured and porous model.

We also proposed a combination of a general linear-slip theory and elastic properties given by Gurevich (2003). For the saturated fractured medium with background porosity, we can still take the compliance matrix as a difference between the compliance matrix of the saturated fractured and porous medium and the saturated host rock. In this work, we investigated the fracture weakness for different directions, and represent the stiffness matrix as sum of the saturated elastic constants and normal fracture weakness for different directions. Assuming the fractures are dipping, we investigated the reflection coefficients variation with incidence angle and azimuth.We observe that an increase in porosity or fracture density make the velocity decreased, and the change is more notable for the horizontal P-wave than vertical P-wave. Both in water saturated and gas saturated fractured rocks, the trend of reflection coefficients changed because of the increase or decrease of the porosity.

In the future, estimation and inversion of physical characteristics of the fractures (e.g., orientation and density of the fractures, and fracture infill) and elastic properties of the host rock will be done.

REFERENCES

Angerer, E., S. A. Horne, J. E. Gaiser, R. Walters, S. Bagala, and L. Vetri, 2002. Characterization of dipping fractures using PS modeconverted data: 72nd Annual International Meeting, SEG, Expanded Abstracts, 1010-1013.

Bakulin A., V. Grechka, and I. Tsvankin, 2000. Estimation of fracture parameters from reflection seismic data-Part 1: HTI model due to a single fracture set: Geophysics, 65, 1788-1802.

Hudson, J.A., 1980. Overall properties of a cracked solid. Math. Proc. Camb. Philos. Soc. 88, 371– 384.

Hudson, J.A., 1981. Wave speeds and attenuation of elastic waves in material containing cracks. Geophys. J. R. Astron. Soc. 64, 133– 150.

Hudson, J. A., 1988, Seismic wave propagation through material containing partially saturated cracks: Geophysical. J. Royal Astronomical, 92, 33-37.

Gassmann, F., 1951. Uber die elastizitat poroser medien. Viertel. Naturforsch. Ges. Zurich 96, 1-23.

Gurevich, B., 2003, Elastic properties of saturated porous rocks with aligned fractures: Journal of Applied Geophysics, 54, 203-218.

Grechka, V., and I. Tsvankin, 2004, Characterization of dipping fractures in a transversely isotropic background: *Geophysical Prospecting*, 52, 1-10.

Mavko, G. M., T. Mukerji, and J. Dvorkin, 2003, The rock physics handbook, tools for seismic analysis in porous media: Cambridge University Press.

Ruger, A., 1998, Variation of P-wave reflecivity with offset and azimuth in anisotropic media; Geophysics, 63, 935-947.

Schoenberg, M., 1980, Elastic wave behavior across linear slip interfaces: Journal of the Acoustical Society of America, 68, 1516-1521.

Schoenberg, M., 1983, Reflection of elastic waves from periodically stratified media with interfacial slip: Geophysical Prospecting, 31, 265-292.

Schoenberg, M., and C. M. Sayers, 1995, Seismic anisotropy of fractured rock: Geophysics, 60, 204-211.

Schoenberg, M., and J. Douma, , 1988, Elastic wave propagation in media with parallel fractures and aligned cracks: Geophysical Prospecting, 36, 571-590.

Shaw, R. K., and M. K. Sen, 2004, Born integral, stationary phase and linearlized reflection coefficients in weak anisotropic media: Geophysical Journal International, 158, 225-238.

Sil, S., and M. K. Sen, 2011, Analysis of fluid substitution in a porous and fractured medium: Geophysics, 76,157-166.

Thomsen, L., 1995, Elastic anisotropy due to aligned cracks in porous rock: Geophysical Prospecting, 43, 805-830.